Strongly Coupled Plasma Physics
S. Ichimaru (Editor)
Elsevier Science Publishers B.V. / Yamada Science Foundation, 1990

OBSERVATION OF CORRELATIONS IN FINITE, STRONGLY COUPLED ION PLASMAS*

J.J. BOLLINGER, S.L. GILBERT, D.J. HEINZEN, W.M. ITANO, and D.J. WINELAND

National Institute of Standards and Technology, 325 Broadway, Boulder, CO 80303

1. INTRODUCTION

We have observed[1] spatial correlations with up to 15 000 Be^+ ions in a Penning trap with a coupling (defined below) of $\Gamma > 100$. These correlations are strongly affected by the boundary conditions and take the form of concentric shells as predicted by computer simulations.[2-4] In this paper we briefly describe the experimental confinement geometry and the method of producing low temperature ions. The relatively large spacings between the ions (~ 20 μm) permit the shells to be directly viewed by imaging the Be^+ laser-induced fluorescence onto a photon-counting camera. Diagnostic techniques capable of measuring the ion diffusion are then discussed. Qualitative observations of the ion diffusion are compared with theoretical predictions.

2. CONFINEMENT GEOMETRY

The Penning trap uses a static, uniform magnetic field and a static, axially symmetric electric field for the confinement of charged particles. The magnetic field, which is directed along the z axis of the trap, provides confinement in the radial direction. The ions are prevented from leaving the trap along the z axis by the electric field. In the work described here, the electric field was provided by three cylindrical electrodes as shown in Fig. 1. The dimensions of the trap electrodes were chosen so that the first anharmonic term (i.e. fourth order term) in the expansion of the trapping potential was zero. Over the region near the trap center, the potential can be expressed (in cylindrical coordinates) as $\Phi \simeq AV_o(2z^2-r^2)$ where $A = 0.146$ cm^{-2}. A background pressure of 10^{-8} Pa($\approx 10^{-10}$ Torr) was maintained by a triode sputter-ion pump. The confinement geometry is similar to that used by the group of the University of California at San Diego (UCSD)[5] with the exception that our trap is smaller than the UCSD traps.

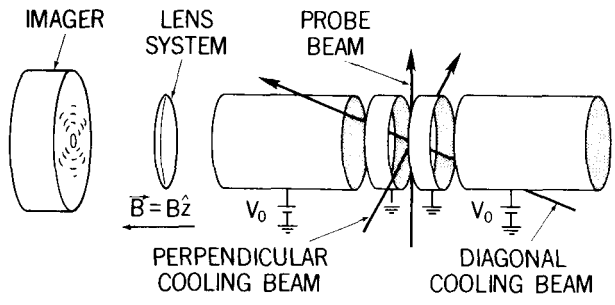

FIGURE 1
Schematic drawing of the trap electrodes, laser beams, and imaging system (not to scale). The overall length of the trap is 10.2 cm. The trap consists of two end cylinders and two electrically connected central cylinders with 2.5 cm inner diameters. Ion clouds are typically less than 1 mm in both diameter and axial length. The diagonal cooling beam crosses the cloud at an angle of 51° with respect to the z axis In the experiments, B = 1.92 T or 0.82 T and V_o ranged between 20 V and 200 V.

The stored ions can be characterized by a thermal distribution where the "parallel" (to the z axis) temperature $T_{\|}$ is approximately equal to the "perpendicular" temperature $T_{\perp}$. This thermal distribution is superimposed on a uniform rotation of the cloud[6-9] at frequency ω which, at the low temperatures of this experiment, is due to the $\vec{E}\times\vec{B}$ drift, where $\vec{E}$ is the electric field due to the trap voltage and the space charge of the ions. In a frame of reference rotating with the ions, the static thermodynamic properties of an ion cloud confined in a Penning trap are identical to those of a one-component plasma (OCP).[7] An OCP consists of a single species of charge embedded in a uniform-density background of opposite charge. For the system of ions in a Penning trap, the trapping fields play the role of the neutralizing background charge. An OCP is characterized by the Coulomb coupling constant,[7,10]

$$\Gamma \equiv q^2/(a_s k_B T),$$

which is a measure of the nearest-neighbor Coulomb energy divided by the thermal energy of a particle. The quantities q and T are the ion charge and temperature. The Wigner-Seitz radius a_s is defined by $4\pi a_s^3 n_0/3=1$, where $-qn_0$ is the charge density of the neutralizing background. In the Penning trap the

background density n_0 depends on the rotation frequency ω and the cyclotron frequency Ω and is given by[6-9]

$$n_0 = m\omega(\Omega-\omega)/(2\pi q^2). \quad (1)$$

3. LASER COOLING AND COMPRESSION

The ion density that can be achieved in a Penning trap is limited by the magnetic field strength that is available in the laboratory. Consequently to obtain large values of Γ and therefore strong couplings, a technique to obtain low ion temperatures is necessary. In our work, radiation pressure from lasers is used to reduce the temperature of the stored ions to less than 10 mK. This technique, known as laser cooling,[11-13] uses the resonant scattering of laser light by atomic particles. The laser is tuned to the red, or low-frequency side of the atomic "cooling transition" (typically an electric dipole transition like the D lines in sodium). Ions with a velocity component opposite to the laser beam propagation ($\vec{k}\cdot\vec{v} < 0$) will be Doppler shifted into resonance and absorb photons at a relatively high rate. Here, $\vec{k}$ is the photon wave vector ($|\vec{k}|=2\pi/\lambda$, where λ is the wavelength of the cooling radiation). For the opposite case ($\vec{k}\cdot\vec{v} > 0$), the ions will be Doppler shifted away from the resonance and the absorption rate will decrease. When an ion absorbs a photon, its velocity is changed by an amount $\Delta\vec{v} = \hbar\vec{k}/m$ due to momentum conservation. Here $\Delta\vec{v}$ is the change in the ion's velocity, m is the mass of the ion, and $2\pi\hbar$ is Planck's constant. The ion spontaneously reemits the photon symmetrically. In particular, when averaged over many scattering events, the reemission does not change the momentum of the ion. The net effect is that for each photon scattering event, the ion's average velocity is reduced by $\hbar\vec{k}/m$. To cool an atom from 300 K to millikelvin temperatures takes typically 10^4 scattering events but, since scatter rates can be 10^8/s, the cooling can be rapid.

In our work with Be^+, the $2s\ ^2S_{1/2} \rightarrow 2p\ ^2P_{3/2}$ "D_2" transition was used as the cooling transition as indicated in Fig. 2. Cooling laser beams were directed both perpendicularly and at an angle with respect to the magnetic field as indicated in Fig. 1. This enabled us to control the cloud size and obtain the lowest possible temperatures.[14,15] The 313 nm radiation required to drive this transition was obtained by frequency doubling the output of a continuous wave, narrow band (3 MHz) dye laser. The 313 nm power was typically 50 μW. The theoretical cooling limit, due to photon recoil effects,[11-13] is given by a temperature equal to $\hbar\gamma/(2k_B)$ where γ is the radiative linewidth of the atomic transition in angular frequency units. For the Be^+ cooling transition ($\gamma = 2\pi \times 19.4$ MHz), the theoretical minimum temperature is 0.5 mK.

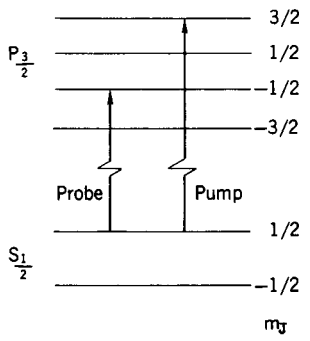

FIGURE 2

Energy level structure of the $^9Be^+$ $^2S_{1/2}$ ground state and the first excited $^2P_{3/2}$ state. The magnetic field splits each state into its m_J sublevels. The laser cooling (pump) and depopulation (probe) transitions are shown.

Laser scattering can also be used to change the angular momentum and compress the stored ion plasma.[8,9] The z component of the canonical angular momentum for an individual ion in the plasma is

$$\ell_z = mv_\theta r + \frac{qBr^2}{2c} . \tag{2}$$

The two terms in Eq. (2) are the ion's mechanical angular momentum and the field angular momentum. The total z component of the angular momentum of the plasma is

$$L_z = m(\Omega/2-\omega)N\langle r^2\rangle. \tag{3}$$

Here N is the total number of ions and $\langle r^2\rangle$ is the mean-squared radius of the plasma. For most of the work described in this paper $\omega \ll \Omega$ and

$$L_z \approx \frac{m\Omega N}{2}\langle r^2\rangle > 0. \tag{4}$$

Therefore the total angular momentum is dominated by the field angular momentum. Suppose the cooling laser beam is directed normal to the z axis but at the side of the plasma which is receding from the laser beam due to the plasma rotation. Because the rotation of the positive ions is in the $-\hat{\theta}$ direction, the torque of the laser on the ions will also be negative. Consequently, angular momentum is removed from the plasma and according to Eq. (4) the radius of the plasma must decrease. In general, the plasma is compressed until the torque due to the cooling laser is balanced by another

external torque. As the radius decreases, the density of the plasma increases.

Even in the absence of external torques, there is a limit to how far the plasma can be compressed. From Eq. (1), the maximum density, known as the Brillouin density, occurs when the rotation frequency $\omega = \Omega/2$. The Brillouin density is given by

$$n_{max} = \frac{m\Omega^2}{8\pi q^2} .$$

We have recently been able to achieve densities at or near the Brillouin limit. In fact we have also been able to achieve rotation frequencies $\omega > \Omega/2$ where according to Eq. (1) the ion density decreases. In these experiments, the temperature was not determined. At the magnetic field of 1.92 T used in some of the work discussed here, the Brillouin density is 1.1×10^9 cm^{-3}. This density with the theoretical minimum 0.5 mK temperature, results in a coupling $\Gamma \sim 5500$. For the work reported here, we have been able to obtain ion temperatures in the 1-10 mK range with densities 5-10 times less than the Brillouin density. This results in couplings Γ of a few hundred.

We measured[8,14,15] the ion density and temperature by using a second laser, called the probe laser, to drive the "depopulation" transition as indicated in Fig. 2. The cooling laser optically pumps the ions into the $^2S_{1/2}$ m_J=+1/2 state.[8] The resonance fluorescence (i.e. laser light scattered by the ions) from this transition is used as a measure of the ion population in the m_J=+1/2 state. The probe laser drives some of the ion population from the $^2S_{1/2}$ m_J=+1/2 state to the $^2P_{3/2}$ m_J=-1/2 state where the ions decay with 2/3 probability to the $^2S_{1/2}$ m_J=-1/2 state. This causes a decrease in the observed ion fluorescence because the $^2S_{1/2}$ m_J=-1/2 state is a "dark" state a (state which does not fluoresce in the cooling laser). The ion temperature is obtained from the Doppler broadening of the resonance lineshape when the probe laser is scanned through the depopulation transition. The ion rotation frequency is measured from the shift in the depopulation transition frequency as the probe laser is moved from the side of the plasma rotating into the laser beam to the side of the plasma rotating with the laser beam. From the measured rotation frequency, the density is calculated from Eq. (1). The measured density and temperature is used to calculate the coupling Γ.

4. OBSERVED CORRELATIONS

With measured couplings $\Gamma > 100$, we anticipate that the ions will exhibit correlated behavior. If the number of stored ions is large enough for

infinite volume behavior, the ions may be forming a bcc lattice.[10] Until now we have cooled and looked for spatial correlations with up to 15 000 Be^+ ions stored in the Penning trap of Fig. 1. A currently unanswered question is how many stored ions are required for infinite volume behavior, i.e. the appearance of a bcc lattice for $\Gamma > 178$. For a finite plasma consisting of a hundred to a few thousand ions, the boundary conditions are predicted to have a significant effect on the plasma state. Simulations involving these numbers of ions in a spherical trap potential predict that the ion cloud will separate into concentric spherical shells.[2-4] Instead of a sharp phase transition, the system is expected to evolve gradually from a liquid state characterized by short-range order and diffusion in all directions, to a state where there is diffusion within a shell but no diffusion between the shells (liquid within a shell, solid-like in the radial direction), and ultimately to an overall solid-like state.[4] These conclusions should apply to a nonspherical trap potential as well if the spherical shells are replaced with shells approximating spheroids. Independent theoretical investigations[16,17] of the nonspherical case support this conjecture.

We have observed shell structures with $^9Be^+$ ions stored in a Penning trap by imaging the laser induced fluorescence from the cooling transition. This technique is sensitive enough to observe the structures formed with only a few ions in a trap.[18-21] About 0.04% of the 313-nm fluorescence from the decay of the $^2P_{3/2}$ state was focused by f/10 optics onto the photocathode of a resistive-anode photon-counting imaging tube (see Fig. 1). The imager was located along the z axis, about 1 m from the ions. The imaging optics was composed of a three-stage lens system with overall magnification of 27 and a resolution (FWHM) of about 5 μm (specifically, the image of a point source when referred to the position of the ions was approximately 5 μm in diameter). Counting rates ranged from 2 to 15 kHz. Positions of the photons arriving at the imager were displayed in real time on an oscilloscope while being integrated by a computer. The probe laser could be tuned to the same transition as the cooling laser and was directed through the cloud perpendicularly to the magnetic field. With the probe laser turned on continuously, the cooling laser could be chopped at 2 kHz (50% duty cycle) and the image signal integrated only when the cooling laser was off. Different portions of the cloud could then be imaged by the translation of the probe beam, in a calibrated fashion, either parallel or perpendicular to the z axis. Images were also obtained from the ion fluorescence of all three laser beams.

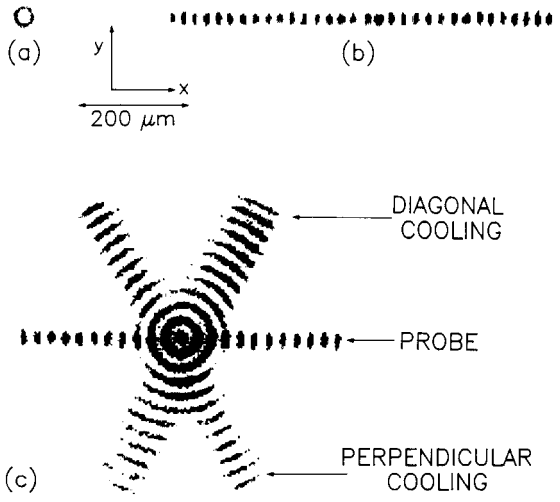

FIGURE 3
Images of shell structures obtained with B = 1.92 T. (a) A single shell in a cloud containing approximately 20 ions. Trap voltage V_0 = 14 V and cloud aspect ratio a_r (axial length/diameter) ≈ 6.5. This image was obtained from the ion fluorescence of the perpendicular and diagonal cooling beams. (b) Sixteen shells (probe-beam ion fluorescence only) in a cloud containing about 15 000 ions with V_0 = 100 V and a_r ≈ 0.8. (c) Eleven shells plus a center column in the same cloud as (b), with V_0 = 28 V and a_r ≈ 2.4. This image shows the ion fluorescence from all three laser beams. Integration times were about 100 s for all images.

We have observed shell structure in clouds containing as few as 20 ions (one shell) and as many as 15 000 ions (sixteen shells). Images covering this range are shown in Fig. 3. Even with 15 000 ions in the trap there is no evidence for infinite volume behavior. We measured the coupling constant Γ for several clouds containing about 1000 ions. Drift in the system parameters was checked by verifying that the same images were obtained before and after the cloud rotation frequency and ion temperatures were measured. Figure 4 shows examples of shell structures at two different values of Γ. The first image is an example of high coupling (Γ ≈ 180) and shows very good shell definition in an intensity plot across the cloud. The second image is an example of lower coupling (Γ ≈ 50) and was obtained with cooling only perpendicular to the magnetic field. Variations in peak intensities equidistant from the z axis are due to signal-to-noise limitations and imperfect alignment between the imager x axis and the probe beam.

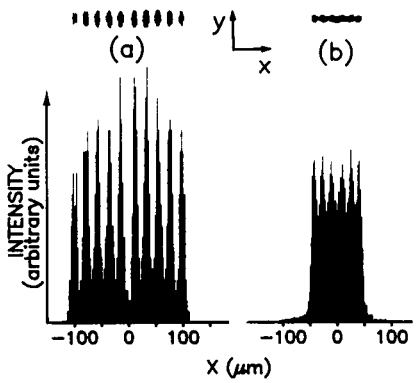

FIGURE 4
Intensity plots along the imager x axis (parallel to the probe beam) through the center of the ion cloud with corresponding images (above). (a) $\Gamma = 180^{+90}_{-70}$ ($T = 6\ ^{+4}_{-2}$ mK, $n_0 \simeq 7\times10^7$ ions cm^{-3}). Cloud aspect ratio $a_r \simeq 3.5$. (b) $\Gamma = 50^{+30}_{-20}$ ($T = 33^{+17}_{-13}$ mK, $n_0 = 2\times10^8$ ions cm^{-3}), $a_r \simeq 5$. The clouds contained about 1000 ions and B = 1.92 T in both cases.

We obtained three-dimensional information on the shell structure by taking probe images at different z positions; two types of shell structure were present under different circumstances. The first type showed shell curvature near the ends of the cloud, indicating that the shells may have been closed spheroids. Shell closure was difficult to verify because of a lack of sharp images near the ends of the cloud where the curvature was greatest. This may have been due to the averaging of the shells over the axial width of the probe beam. In the other type of shell structure, it was clear that the shells were concentric cylinders with progressively longer cylinders near the center. An example of these data is shown in Fig. 5. Other evidence for cylindrical shells was obtained from the observation that shells in the diagonal-beam images occurred at the same cylindrical radii as those from the perpendicular beams. This can be seen in the three-beam images such as that shown in Fig. 3(c). Systematic causes of these two different shell configurations have not yet been identified.

One comparison which can be made between the theoretical calculations and our experimental results is the relationship between the number of shells and the number of ions, N, in a cloud. For a spherical cloud, two independent approaches[2,22] estimate $(N/4)^{1/3}$ and $(3N/4\pi)^{1/3}$ shells. For the nearly spherical cloud of Fig. 3(b) ($N \simeq 15\ 000$), these formulae predict 15.5 and

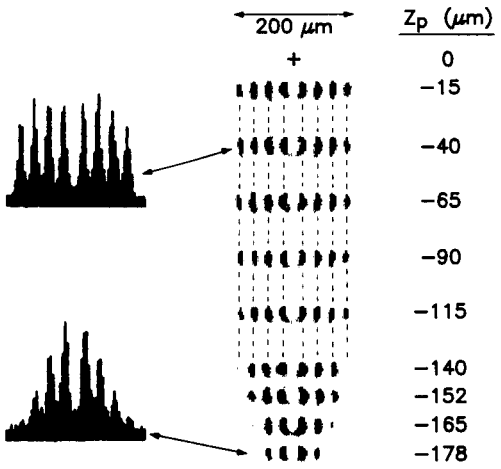

FIGURE 5
Data showing evidence for concentric cylindrical shells. On the right is a series of images obtained with the probe beam for different z positions z_p of the probe beam (lower half of the cloud only). Intensity plots for z_p = -40 μm and z_p = -178 μm are shown on the left. The cloud aspect ratio a_r was about 1.9 and B ≃ 1.92 T.

15.3 shells and we measure 16. At present, it is difficult to make further quantitative comparisons between our data and the theoretical calculations. For example, there is substantial uncertainty in our measurement of Γ due to uncertainty in the temperature measurement. Our data do agree qualitatively with the simulations with the exception, in some cases, of the presence of an open-cylinder shell structure as opposed to the predicted closed spheroids. Shear (that is, different rotation frequencies) between the shells could possibly account for this discrepancy. In our experiment, shear could be caused by differential laser torque or the presence of impurity ions.[8] For the data here, we have determined that the rotation frequency does not vary by more than 30% across the cloud.

5. ION DIFFUSION

The probe laser can be used to optically tag ions and observe the ion diffusion.[14] With the probe laser tuned to the depopulation transition (see Fig. 2), ions in the path of the probe laser beam are put into the "dark" m_J= -1/2 ground state. These ions will not fluoresce when they pass through the cooling laser until they are optically pumped back into the m_J=+1/2 ground state. This repumping time is typically on the order of 1.0 s. By pulsing the probe laser on and measuring the length of time it takes the dark ions to

diffuse from the probe beam to the cooling laser beam, it should be possible to measure the ion diffusion. By directing the probe laser beam to the radial edge of the plasma so that only the outer shell is intersected by the probe beam, it should be possible to observe the diffusion of ions in the radial direction or between shells. By directing the probe beam to the axial edge of the cloud it should be possible to observe the diffusion of the ions in the axial direction or within a shell. According to the simulations of Dubin and O'Neil,[4] for intermediate values of the coupling ($\Gamma \sim 100$) we expect to observe that the diffusion between shells is much slower than the ion diffusion within a shell (solid-like behavior between shells, liquid-like within a shell). As the temperature is lowered and the coupling Γ increases, the diffusion within a shell should smoothly slow down. At high enough couplings (i.e. $\Gamma > 400$) the diffusion should be very slow both between and within shells, indicative of solid-like behavior.

We have qualitatively observed the ion diffusion at intermediate values of Γ ($\Gamma \sim 100$-200). We observed that the diffusion of ions between shells is slow compared to the optical repumping time ($\sim$ 1 s) but that the diffusion within a shell (i.e. from the axial end of a shell to the $z = 0$ plane) is fast compared to this repumping time. We have also observed states with higher couplings (the couplings Γ were not measured) where the diffusion of ions both between and within a shell was slow compared to the optical repumping time. In the future we plan to make quantitative measurements of the ion diffusion.

ACKNOWLEDGEMENT

We gratefully acknowledge the support of the U.S. Office of Naval Research and the Air Force Office of Scientific Research. We thank M. Raizen and F. Moore for carefully reading the manuscript.

REFERENCES

1) S.L. Gilbert, J.J. Bollinger, and D.J. Wineland, Phys. Rev. Lett. 60 (1988) 2022.

2) A. Rahman and J.P. Schiffer, Phys. Rev. Lett. 57 (1986) 1133; J.P. Schiffer, Phys. Rev. Lett. 61 (1988) 1843.

3) H. Totsuji, in Strongly Coupled Plasma Physics, eds. F.J. Rogers and H.E. DeWitt (Plenum, New York, 1987) pp. 19-33.

4) D. Dubin and T. O'Neil, Phys. Rev. Lett. 60 (1988) 511.

5) C.F. Driscoll, J.H. Malmberg, and K.S. Fine, Phys. Rev. Lett. 60 (1988) 1290; J.H. Malmberg and J.S. deGrassie, Phys. Rev. Lett. 35, 577 (1975).

6) T.M. O'Neil, in Non-Neutral Plasma Physics, eds. C.W. Roberson and C.F. Driscoll (American Institute of Physics, New York, 1988) pp. 1-25.

7) J.H. Malmberg and T.M. O'Neil, Phys. Rev. Lett. 39 (1977) 1333.

8) L.R. Brewer, J.D. Prestage, J.J. Bollinger, W.M. Itano, D.J. Larson, and D.J. Wineland, Phys. Rev. A38 (1988) 859.

9) D.J. Wineland, J.J. Bollinger, W.M. Itano, and J.D. Prestage J. Opt. Soc. Am. B2 (1985) 1721.

10) S. Ichimaru, H. Iyetomi, and S. Tanaka, Phys. Rep. 149 (1987) 91 and references therein.

11) D.J. Wineland and W.M. Itano, Phys. Rev. A20 (1979) 1521.

12) W.M. Itano and D.J. Wineland, Phys. Rev. A25 (1982) 35.

13) D.J. Wineland and W.M. Itano, Phys. Today 40(6) (1987) 34; S. Stenholm, Rev. Mod. Phys. 58 (1986) 699.

14) L.R. Brewer, J.D. Prestage, J.J. Bollinger, and D.J. Wineland, in Ref. 3), pp. 53-64.

15) J.J. Bollinger and D.J. Wineland, Phys. Rev. Lett. 53 (1984) 348.

16) J.P. Schiffer, Argonne Natl. Lab., Argonne, IL, private communication.

17) D.H.E. Dubin, Dept. of Physics, UCSD, La Jolla, CA, private communication.

18) F. Diedrich, E. Peik, J.M. Chen, W. Quint, and H. Walther, Phys. Rev. Lett. 59 (1987) 2931.

19) D.J. Wineland, J.C. Bergquist, W.M. Itano, J.J. Bollinger, and C.H. Manney, Phys. Rev. Lett. 59 (1987) 2935; D.J. Wineland, W.M. Itano, J.C. Bergquist, S.L. Gilbert, J.J. Bollinger, and F. Ascarrunz, in Ref. 6), pp. 93-108.

20) J. Hoffnagle, R.G. DeVoe, L. Reyna, R.G. Brewer, Phys. Rev. Lett. 61 (1988) 255.

21) Th. Sauter, H. Gilhaus, I. Siemers, R. Blatt, W. Neuhauser, P.E. Toschek, Z. Phys. D10 (1988) 153.

22) D.H.E. Dubin, Phys. Rev. A40 (1988) 1140.